Automated Identification of Cardiac Signals after Blind Source Separation for Camera-Based Photoplethysmography

Daniel Wedekind, Hagen Malberg, Sebastian Zaunseder

Institute of Biomedical Engineering
Faculty of Electrical and Computer Engineering
TU Dresden
Dresden, Germany
daniel.wedekind@tu-dresden.de

Frederik Gaetjen, Klaus Matschke, Stefan Rasche

Herzzentrum Dresden GmbH
University Hospital Carl Gustav Carus Dresden
TU Dresden
Dresden, Germany
stefan.rasche@mailbox.tu-dresden.de

Abstract – **In the field of camera-based photoplethysmography the application of blind source separation (BSS) techniques has extensively stressed to cope with frequently occurring artifacts and noise. Although said techniques can help to extract the cardiac component from a mixture of input sources, permutation indeterminacy inherit to BSS techniques often introduces inaccuracies or requires manual intervention. The current contribution focuses on methods to automatically select the cardiac component from the output of BSS techniques applied to camera-based photoplethysmograms. To that end, we propose simple Markov models to describe and subsequently identify cardiac components. It is shown that good results can be obtained by combining different simple Markov models.**

Keywords – camera-based photoplethysmography, blind source separation, independent component analysis, principal component analysis, permutation indeterminacy, markov model

I. INTRODUCTION

The contact-less acquisition of vital signs allows for the implementation of novel clinical and out-of-hospital applications. Various systems and techniques for contactless measurements have been introduced in the last years. Amongst such approaches camera-based monitoring is one promising solution.

The acquisition of the cardiac pulse by using near infrared cameras was firstly demonstrated by Huelsbusch et al. 2002 [1]. Since then many researchers have addressed the camera-based photoplethysmography most often to capture the heart rate [2], [3],[4],[5].

Since the camera-based photophlethysmogram (cbPPG) strongly suffers from artifacts induced by motion and changes in light conditions, elaborated image and signal processing techniques are required to make use of the cbPPG under real world conditions. In that context, the application of blind source separation (BSS) algorithms to extract the cardiac pulse from video recordings has been extensively stressed. BSS is intended to separate the desired signal content (the cardiac pulse) from noise and artifacts by means of decorrelation and utilization of statistical independence.

Principal Component Analysis (PCA) and Independent Component Analysis (ICA) [6] as typical BSS techniques have been applied to the cbPPG. Common camera-based applications [4], [7], [8], [9], [10], [11], [12], [13] input segments of different color channels, typically RGB, extracted from regions of interest (ROI) including the complete subjects' face or parts of it to the PCA or the JADE ICA [14]. Also the FastICA algorithm [15] was applied to RGB signals [12], [16] and achieved a slightly better performance in comparison to other ICA algorithms [16]. Tsouri et al., in turn, input RGB information of a face ROI to the constrained ICA and successively embed sines at assumed heart rates as constraint to select the most probable heart rate [17]. A combination of spectra from ICA outputs and its underlying RGB signals in terms of a support vector regression for heart rate estimation is proposed in [18]. A monochrome cbPPG extracted from the forehead ROI is used as input for spatio-temporal ICA in [18]. Motion information in terms of trajectories of tracked face features are processed with PCA in [19] to extract the heart rate. Even in the processing of classic PPG (finger clip), FastICA algorithms have been applied for the purpose of motion compensation. Again, temporal segments of different wavelengths (this time near infrared and red) are fed into ICA [20], [21].

One major drawback of ICA's application is the permutation indeterminacy of the output components, i.e. the components given by the algorithm are of random order. Even PCA, which generates an output order regarding the explained variance by the components [6], cannot guarantee a fixed position of the component belonging to the cardiac pulse in presence of noise. Despite its importance for practical applications, an automated selection of the desired component has been rarely addressed. Some proposals simply select a fixed (namely the second) component after transformation of the RGB channels [4], [9], [10]. Only one of these works briefly assesses the results obtained for this selection [10]. Some approaches address a distinct peak in the spectrum (caused by the cardiac pulse) by selecting the component with the maximum peak [7], [1], [13], [16] or the maximum spectral signal-to-noise ratio (SNR) [3], respectively. Alternatively, component selection based on cross correlation with an assumed heart rate from the processing was described in [22]. Others neglect an automated component selection [12], [19], [20], exclude the artifact component instead of selecting the pulse component [21] or avoid a direct

422

component selection by addressing a different postprocessing issue [17], [18]. Another approach assesses the similarity of the de-mixing matrix (as one ICA result) to the expected composition of a pulse component from the RGB signals [8].

The scope of this contribution is the investigation of automated component selection algorithms after applying PCA and ICA to the cbPPG. We compare the proposed idea of evaluating output components' spectra [3], [7], [11], [13], [16] with an alternative approach to component selection based on Markov models. Thereby, Markov models, that for example have been applied to classification of cardiac rhythm [23], are intended to automatically classify the most probable cardiac component inside the PCA/ICA output based on simple features from time and frequency domain.

II. MATERIALS AND METHODS

A. Data Recording and Selection

Video data was recorded using an industrial camera (IDS UI-3370CP-C-HQ, 100 fps, 420x320 pixels, RGB 3x12 bit). The camera was placed at a distance of approximately 60 cm to patients faces. See figure 1 for a video frame example. For illumination, a fluorescent light source and natural light was used respectively. 18 recordings (13 male, 5 female; 30 minutes per recording) of resting cardiovascular patients in a supine position during recovery after heart surgery were selected from a larger collective. Electrocardiogram (ECG) and finger PPG were simultaneously recorded at 100 Hz as reference. Written informed consent was obtained from all patients. The study was approved by the Ethics Committees of Technische Universität Dresden.

In order to use only suitable data for further analysis, we restricted our analysis to data segments which showed good quality on the reference PPG and that did not contain severe cardiac disorders. A total of 22000 s video data was selected (average length 1200 ± 400 s per patient). Since the selection did not consider video quality, video segments containing slight patient motion as well as lightning inadequacies (changes or insufficient lightning) were included

B. Data Extraction

Based on the prerequisite of a linear mixing process [6] of desired signals with noise and artifacts in standard PCA/ICA, we restricted our cbPPG extraction from RGB video data to one single wavelength. This is a major difference compared to proposed ICA applications on cbPPG [4], [7], [9], [10], [11], [12], [13], [16]. In particular, we expect the wavelength-dependent penetration depth into human skin [1] to introduce nonlinear mixing behavior which might affect the performance of BSS algorithm negatively. Due to advantageous absorption properties, the green channel was selected as the channel to be used for our analysis [2]. Patients were expected to lie motionless due to anesthesia. We therefore manually selected three static 32 x 32 pixel ROIs on each patients forehead (see figure 1 for an example), which served as the basis for signal extraction within the videos. The cbPPG was extracted from each ROI by averaging its pixel values for consecutive frames to obtain a time series (see figure 2 for an example) [1].

Fig. 1. Sample patient video frame showing three exemplary forehead ROIs for cbPPG extraction using the green color channel.
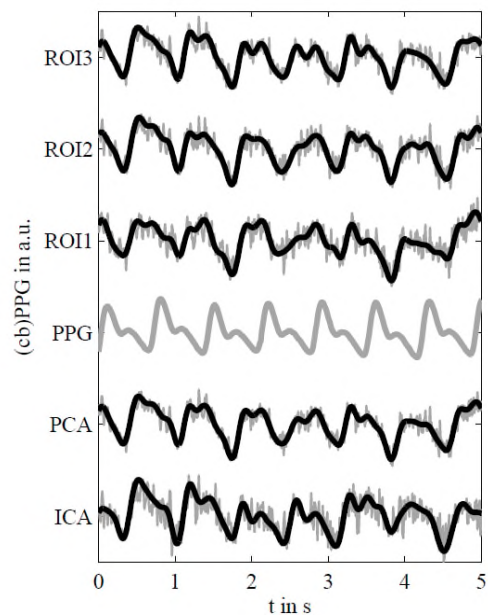

Fig. 2. Sample cbPPG excerpt showing signals extracted from three forehead ROIs with corresponding PPG and BSS components selected by model MM2.

C. Data Processing

The preselected signal excerpts were further processed in subsegments of 10 s length each (overlap 1.5 s). Each 10 s cbPPG signal from ROIn (with n = 1,2,3) was normalized by subtracting its mean and division through its standard deviation. Every subset of three cbPPG signals subsequently served as input to applied BSS techniques, namely PCA and FastICA (symmetric use, general-purpose tanh-nonlinearity [15]). Consequently, we obtained three output components (y_{PCAn}, y_{ICAn}, n = 1,2,3) for each subsegment. We then estimated the SNR of every output component similar to [7]. To that end, the heart rate from the reference ECG (calculated from the current average beat-to-beat-distances) was used to find the maximum peaks in the amplitude spectra $S(f)$ of the components. A binary mask BM containing the spectral

indices belonging to the frequency which is considered as signal frequency f_{si} (heart rate) as well as its first harmonic ($\pm$ 5 beats per minute (bpm) or $\pm$ 0.083 Hz) is generated according to:

$$BM^{f_{si}}(f) = \begin{cases} 1 & if \quad f \in [f_{si} \pm 5bpm] \\ 1 & if \quad f \in [2f_{si} \pm 5bpm] \\ 0 & otherwise \end{cases} \quad (1)$$

A SNR is hereafter calculated as [7]:

$$SNR^{f_{si}} = 10 \cdot \log_{10} \frac{\sum_{f=30bpm}^{240bpm} \left(BM^{f_{si}}(f) \cdot S(f)\right)^2}{\sum_{f=30bpm}^{240bpm} \left((1-BM^{f_{si}}(f)) \cdot S(f)\right)^2} \quad (2)$$

The $SNR^{f_{si}}$ of the cardiac pulse (f_{si} = heart rate) serves as measure of quality of the output components. An automated channel selection is desired to select the channel of maximum $SNR^{f_{si}}$ among the output components.

D. Output Component Selection Based on SNR

Since in reported applications of BSS on cbPPG a spectral selection of the desired cardiac component is proposed [3], [7], [11] we implemented a component selection based on the SNR. Despite deriving the heart rate from the reference signal the maximum peak of $S(f)$ inside a plausible heart rate range (30-240 bpm or 0.5-4 Hz, [7], [24]) is utilized as f_{si}. The calculation of the SNR is then done according to equation (1) and (2) and the component with maximum $SNR^{f_{si}}$ is selected. In the following, we denote the automated component selection without reference as selfSNR.

E. Output Component Selection Based on Markov Models

A Markov model (MM) is a stochastic model characterized by the assumptions that future states depend only on the present state and are independent of any preceding state [25]. We chose this model type for its robustness: typical component selection methods, for example based on the SNR, use the entire characteristics of a channel/component. Thus, they can get misled by intermittent distortions of the tracked characteristics (like the spectral cardiac pulse), which were not properly separated by BSS routines. Developing a feature, and hence a state, which is recurrent within one component of for example 10 s duration may allow even short but typical segments to dominate the component selection. Moreover, a Markov model can be based on simple and easy accessible features which makes MM reasonable to practical applications and improve the comprehensibility of their behavior.

We developed three Markov models to identify cardiac pulses in processed cbPPG on the basis of the reference PPG subsegments (10 s length each, 1.5 s overlap). The PPG subsegments were obtained according to the data selection depicted above. These three models are intended to assess different time and frequency domain characteristics of the PPG (with application to PCA/ICA components of the cbPPG). To allow for patient-dependent changes in morphology of the PPG waveform [26], we considered a frequency range of the PPG which exceeds the expected heart frequency range. In particular, we chose two different frequency ranges, one wide (0.25 - 7 Hz) and one narrow (0.5 - 5 Hz) for each model. The frequency restriction thereby directly affects the PPG/cbPPG characteristic to be evaluated by the model. The frequency range was applied by bandpass filtering (5th order Butterworth) the PPG before training the model. The same bandpass filtering was applied to the PCA/ICA components before classification of the most suitable component. To generate a Markov model embedding the undesired characteristic (the unwanted component), we additionally trained every model with the same quantitative amount of random generated (normally distributed) signals. The statistics of the random signal assessment in combination with the PPG statistics and its transition probabilities p_{ij} are used to calculate the transition likelihood L_{ij} for each state pair (i,j), which is similar to [23]:

$$L_{ij} = \log_{10}\left(p_{ij,random} / p_{ij,PPG}\right) \quad (3)$$

Thus, the negative elements of L_{ij} are more likely to occur in PPG than in random signals. This property is used to classify the PCA/ICA output components of the cbPPG. In particular, state transitions according to the models are detected and a time series z_L of consecutive elements of L_{ij} is built for each output component. The average of every components' z_L is compared and the most negative $\overline{z_L}$ is chosen to determine the desired cardiac pulse component.

1) MM Assessing the Time Course. The first model (MM1) assesses amplitude changes in the time course of the PPG/cbPPG. Therefore, instantaneous slopes m obtained by directly connecting curve points are calculated and classified into states according to:

1. $0 \leq m < 1$
2. $m \geq 1$
3. $0 > m > -1$
4. $m \leq -1$

Having a discrete PPG/cbPPG time series $y_{PPG}(k)$ and the corresponding time stamps $t_{PPG}(k)$, the new slope estimate

$$m_{new} = \frac{y_{PPG}(k+n) - y_{PPG}(k)}{t_{PPG}(k+n) - t_{PPG}(k)} \quad with \quad \begin{matrix} n = n+1 \\ k = const \end{matrix} \quad (4)$$

is updated as long as the absolute difference between the preceding slope estimate m_{old} and the new slope m_{new} is smaller than 50%. If this boundary is exceeded, the slope is classified according to the specifications above and stored as reached state. A new slope estimation is attached after updating $k=k+n$ and resetting $n=1$. See figure 3 for a slope classification example on a PPG.

2) MM Assessing the Autocorrelation Function. The second model (MM2) assesses the periodicity of the signal by its autocorrelation function. In particular, the autocorrelation function of a periodic function itself comprises periodicity of decreasing amplitude with increasing time lag τ.
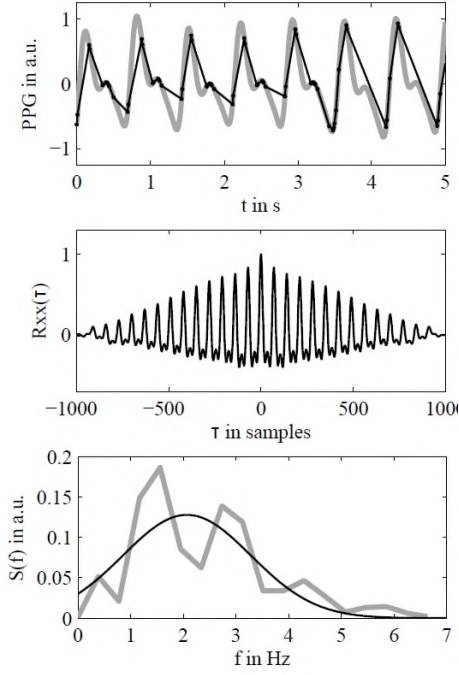
Fig. 3. Upper plot: sample PPG excerpt (grey) with indicated MM generated slope assessment (black), center plot: sample autocorrelation function *Rxx* of the shown PPG (upper plot, but underlying full 10 s subsegment length), lower plot: amplitude spectrum *S(f)* (grey) of the first two seconds of the shown PPG (upper plot) and fitted gaussian (black)

We track this behavior for a PPG/cbPPG (see figure 3 for an autocorrelation function example of a PPG) by using a two-state model evaluating consecutive local extrema (amplitude) of the autocorrelation function. Namely, we start from time lag $\tau = 0$ and detect amplitudes of consecutive local maxima at τ_n, τ_{n+1},... (respectively minima) and assess their temporal behavior:

1. local maxima at $|\tau_n| \geq$ local maxima at $|\tau_{n+1}|$ respectively local minima at $|\tau_n| \leq$ local minima at $|\tau_{n+1}|$
2. otherwise

3) MM Assessing the Spectral Course. The third model (MM3) assesses the changes in the amplitude spectrum by calculating a short time fourier transform, i.e. windowed FFTs. The spectrum at each time is simply described by a single gaussian fitted into the spectrum (see figure 3 for an example). The parameters mean μ_f and standard deviation σ_f of this gaussian are evaluated to track a change in the spectrum by shifting the underlying window. We chose the window length to stretch over 200 samples (including Hanning windowing), i.e. two seconds, and a translation by 25 samples. This dimension was intended to edge the expected heart rate range (0.5-4 Hz). The model states are defined by the changes of μ_f and σ_f caused by the recalculation in the k-th window. We combined the changes of both fitting parameters to one single change $\Delta_{\overline{gauss}}$ in terms of (k > 1):

$$\Delta_{\overline{gauss}}(k) = \frac{1}{2}\left(\frac{\mu_f(k) - \mu_f(k-1)}{|\mu_f(k-1)|} + \frac{\sigma_f(k) - \sigma_f(k-1)}{|\sigma_f(k-1)|} \right) \quad (5)$$

and derived a three state model according to:

1) $\Delta_{\overline{gauss}} \leq -5\%$

2) $-5\% < \Delta_{\overline{gauss}} < -5\%$

3) $\Delta_{\overline{gauss}} \geq -5\%$

F. Evaluation of Selection Performance

Since every cbPPG PCA/ICA output component is assessed with one $SNR^{f_{si}}$ (f_{si} = heart rate) for each 10 s subsegment, we applied selfSNR (f_{si} = maximum peak) component selection as well as three Markov model component selection for both frequency ranges to each output component set (see figure 2 for an example of the MM2 selection after BSS). In the following we compare the component with maximum $SNR^{f_{si}}$ (maxSNR, f_{si} = heart rate) with the automated component selections and assess the portion in which the automated selection yields the best possible SNR. A theoretical optimum of combining two or three Markov models (inside one frequency range) for the selection was also assessed by estimating synergistic selection potentials.

III. RESULTS

A. Trained Component Assessment Matrices L_{ij}

Subsequently, the matrices L_{ij} as the result of the Markov model training using the reference PPG are depicted. They represent the likelihood of a state transition from a present state i (column) to a future state j (row). Negative values indicate a behavior typical for PPG, whereas positive values indicate state transitions atypical for PPG. Typical behavior thereby refers to the comparison with a normally distributed random signal used for training of the non-PPG signal.

1) MM1: wide band model (0.25-7 Hz) $L1w_{ij}$ and narrow band model (0.5-5 Hz) $L1n_{ij}$:

$$L1\omega_{ij} = \begin{vmatrix} -0.23 & 0.18 & 0.05 & 0.57 \\ 0.44 & -0.02 & 0.12 & 0.36 \\ 0.19 & 0.02 & -0.07 & -0.27 \\ -0.41 & -0.08 & 0.13 & -0.23 \end{vmatrix}$$

$$L1n_{ij} = \begin{vmatrix} -0.29 & 0.24 & 0.14 & 0.60 \\ 0.60 & -0.03 & 0.14 & 0.83 \\ 0.18 & 0.03 & -0.08 & -0.30 \\ -0.46 & -0.01 & 0.30 & -0.41 \end{vmatrix}$$

2) MM2: wide band model (0.25-7 Hz) *L2w_{ij}* and narrow band model (0.5-5 Hz) *L2n_{ij}*:

$$L2\omega_{ij} = \begin{vmatrix} -0.21 & -0.18 \\ 0.27 & 0.87 \end{vmatrix} \quad L2n_{ij} = \begin{vmatrix} -0.29 & -0.18 \\ 0.33 & 02.15 \end{vmatrix}$$

3) MM3: wide band model (0.25-7 Hz) *L3w_{ij}* and narrow band model (0.5-5 Hz) *L3nij*:

$$L3\omega_{ij} = \begin{vmatrix} 0.18 & 0.44 & -0.05 \\ -0.56 & -0.40 & -0.21 \\ 0.17 & 0.19 & 0.16 \end{vmatrix} \quad L3n_{ij} = \begin{vmatrix} 0.68 & 0.65 & -0.21 \\ -0.76 & -0.48 & -0.27 \\ 0.25 & 0.33 & 0.67 \end{vmatrix}$$

B. Component Selection Performance

Table I (PCA) and table II (ICA) show the results of the performance of each component selection method (selfSNR,MM) regarding its ability to choose the maxSNR component after cbPPG processing.

It can be noted that none of the Markov models alone achieves a better selection performance than the component selection based on SNR (selfSNR). On the other hand, any combination of two or three Markov models shows higher detection rates than selfSNR. Quantitatively, SNR reaches selection rates of about 70% on average, whereas the best combination of MM (using all three models) shows a selection performance of about 85% for ICA and PCA.

Component selection after ICA in general shows a poorer performance than after PCA despite the single model selection using the frequency course MM3. The best single model selection independent of PCA/ICA is reached by the simplest model utilizing the fewest model states MM2. This is underlined by the fact that the two-model selection without MM2 achieves the poorest performance out of the possible model combinations.

Applying a narrower bandpass filter to train the models and classify the components respectively, in general comes to improving the component selection performance. One solitary exception is given by the single model selection using MM1. Nevertheless, the application of the narrow bandpass filter used here was not able to facilitate a better single Markov model selection performance than using selfSNR.

IV. DISCUSSION

As our results indicate the component selection aiming at an optimal SNR is not solved by existing approaches, which yield only $\approx$ 70%. We show that combining simple Markov models can contribute to an improvement (up to $\approx$ 85%) of the selection performance. However, an automated fusion of several Markov models was not in the scope of this work and has to be addressed in future works to exploit the potential of Markov models. Moreover, the automated selection of the maxSNR component may not be necessary for every practical task, for example estimating the correct heart rate. Thus, a correct heart rate may also be accessible from other components. A more detailed investigation of component selection algorithms should include an analysis of the influence of the component selection on later processing steps and results, for example assessing the heart rate error after applying a certain estimation method.

TABLE I.   MEANS (MEDIANS) AND STANDARD DEVIATIONS (STMCSR) (IN %) OF THE MAXSNR COMPONENT SELECTION RATES (MMCSR) BY USING AUTOMATED COMPONENT SELECTIONS (SELFSNR, MARKOV MODELS MM1-3 AND MODEL COMBINATIONS) AFTER PCA.

PCA								
component selection	selfSNR		MM1		MM2		MM3	
MM frequency range	mMCSR	stMCSR	mMCSR	stMCSR	mMCSR	stMCSR	mMCSR	stMCSR
wide (0.25 - 7 Hz)	71.91 (73.94)	21.19	54.19 (55.27)	17.68	61.05 (59.21)	21.20	38.22 (36.27)	10.54
narrow (0.5 - 5 Hz)			52.62 (56.22)	16.72	67.45 (64.20)	19.36	48.34 (44.74)	14.46
component selection	MM1+2		MM1+3		MM2+3		MM1+2+3	
MM frequency range	mMCSR	stMCSR	mMCSR	stMCSR	mMCSR	stMCSR	mMCSR	stMCSR
wide (0.25 - 7 Hz)	76.74 (78.26)	15.17	72.71 (74.36)	11.46	74.13 (72.37)	13.81	85.58 (86.73)	9.42
narrow (0.5 - 5 Hz)	80.05 (84.26)	14.46	74.35 (76.90)	13.69	79.65 (79.42)	12.64	87.67 (91.44)	9.30

TABLE II.   MEANS (MEDIANS) AND STANDARD DEVIATIONS (STMCSR) (IN %) OF THE MAXSNR COMPONENT SELECTION RATES (MMCSR) BY USING AUTOMATED COMPONENT SELECTIONS (SELFSNR, MARKOV MODELS MM1-3 AND MODEL COMBINATIONS) AFTER ICA.

ICA								
component selection	selfSNR		MM1		MM2		MM3	
MM frequency range	mMCSR	stMCSR	mMCSR	stMCSR	mMCSR	stMCSR	mMCSR	stMCSR
wide (0.25 - 7 Hz)	69.58 (67.09)	20.14	35.28 (35.28)	6.37	53.89 (48.74)	18.07	39.12 (37.18)	11.32
narrow (0.5 - 5 Hz)			32.96 (34.14)	6.56	63.36 (62.10)	17.77	50.05 (47.82)	13.88
component selection	MM1+2		MM1+3		MM2+3		MM1+2+3	
MM frequency range	mMCSR	stMCSR	mMCSR	stMCSR	mMCSR	stMCSR	mMCSR	stMCSR
wide (0.25 - 7 Hz)	71.30 (69.23)	11.61	60.26 (59.40)	8.43	70.24 (69.50)	12.50	81.37 (80.89)	7.92
narrow (0.5 - 5 Hz)	75.62 (73.25)	11.30	66.02 (63.96)	9.34	77.93 (75.83)	10.98	84.94 (83.42)	7.05

The evaluation of the influence of two different bandpass filters on the model performance shows that increased smoothing of the model input not necessarily contributes to an increased selection performance. A filter beneficial for extraction of features for MM2 and MM3 is found to simultaneously decrease the performance of MM1. Thus, a proper feature characterization and its state extraction needs to be considered during each model development. A selection performance increase in turn with for example a decreasing state transition likelihood of an anyway negative transition likelihood could indicate a beneficial use of the applied changes in preprocessing. This could be observed for several state transitions in MM2 and MM3. MM1 by contrast shows, that this behavior found in some of the state transitions not necessarily comes with a performance increase but highlights the apparent influence of other state transitions of smaller value. Suchlike examinations could be used to optimize the performance of single models. Moreover, the quantity of transition likelihoods compared to each other could be useful to identify characteristic state transitions and thus, characteristic behavior of the desired content.

Furthermore, the application of normally distributed random signals for training the undesired (non-PPG) signal behavior have to be assessed in future model developments. A better characterization of undesired content for example by assessing the detailed behavior of PCA/ICA output components without any cardiac pulse content may contribute in a clarification of the state transition likelihoods. Moreover, hidden Markov models [25] could help identifying states and models beyond a straightforward signal description.

CONCLUSION

The presented work demonstrates that simple modeling by means of MM can serve as basis to select the most suitable component after applying BSS techniques. Future works must address techniques to automatically combine the output of several MM to exploit the full potential of that approach.

ACKNOWLEDGMENT

REFERENCES

[1] M. Huelsbusch and V. Blazek, "Contactless Mapping of Rhythmical Phenomena in Tissue Perfusion Using PPGI," in Proceedings of the Medical Imaging 2002 (SPIE 4683), San Diego, USA, 2002, pp. 110–117.

[2] W. Verkruysse, L. Svaasand, and J. Stuart Nelson, "Remote plethysmographic imaging using ambient light," Optics Express, vol. 16, no. 26, pp. 21 434–21 445, 2008.

[3] G. Balakrishnan, F. Durand, and J. Guttag, "Detecting Pulse from Head Motions in Video," in Proceedings of the IEEE CVPR, Portland, USA, 2013, pp. 3430–3437.

[4] M. Poh, D. McDuff, and R. Picard, "Non-contact, automated cardiac pulse measurements using video imaging and blind source separation," Optics Express, vol. 18, no. 10, pp. 10 762–10 774, 2010.

[5] H. Wu, M. Rubinstein, E. Shih, J. Guttag, F. Durand, and W. Freeman, "Eulerian video magnification for revealing subtle changes in the world," ACM Transactions on Graphics, vol. 31, no. 4, pp. 1–8, 2012.

[6] P. Comon, "Independent component analysis, A new concept?" Signal Processing, vol. 36, no. 3, pp. 287–314, 1994.

[7] G. de Haan and V. Jeanne, "Robust pulse-rate from chrominance-based rPPG," IEEE Transactions on Biomedical Engineering, vol. 60, no. 10, pp. 2878–2886, 2013.

[8] G. de Haan and A. van Leest, "Improved motion robustness of remote-PPG by using the blood volume pulse signature." Physiological measurement, vol. 35, no. 9, pp. 1913–1926, 2014.

[9] B. Holton, K. Mannapperuma, P. Lesniewski, and J. Thomas, "Signal recovery in imaging photoplethysmography." Physiological measurement, vol. 34, no. 11, pp. 1499–1511, 2013.

[10] S. Kwon, H. Kim, and K. Suk Park, "Validation of heart rate extraction using video imaging on a built-in camera system of a smartphone," in Proceedings of 34th IEEE EMBS, San Diego, USA, 2012, pp. 2174–2177.

[11] M. Poh, D. McDuff, and R. Picard, "Advancements in Noncontact, Multiparameter Physiological Measurements Using a Webcam," IEEE Trans. Biomed. Eng., vol. 58, no. 1, pp. 7–11, 2011.

[12] M. Lewandowska, J. Ruminski, T. Kocejko, and J. Nowak, "Measuring pulse rate with a webcam: A non-contact method for evaluating cardiac activity," in Proceedings of the FedCSIS, Szczecin, Poland, 2011, pp. 405–410.

[13] D. McDuff, S. Gontarek, and R. Picard, "Remote Detection of Photoplethysmographic Systolic and Diastolic Peaks Using a Digital Camera," IEEE Transactions on Biomedical Engineering, vol. 61, no. 12, pp. 2948–2954, 2014.

[14] J. Cardoso, "High-order contrasts for independent component analysis." Neural Computation, vol. 11, no. 1, pp. 157–192, 1999.

[15] A. Hyva̅rinen, "Fast and Robust Fixed-Point Algorithms for Independent Component Analysis," IEEE Transactions on Neural Networks, vol. 10, no. 3, pp. 626–634, 1999.

[16] E. Christinaki, G. Giannakakis, F. Chiarugi, M. Pediaditis, and G. Iatraki, "Comparison of Blind Source Separation Algorithms for Optical Heart Rate Monitoring," in Proceedings of the 4th Mobihealth, Athens, Greece, 2014, pp. 339–342.

[17] G. Tsouri, S. Kyal, S. Dianat, and L. Mestha, "Constrained independent component analysis approach to nonobtrusive pulse rate measurements." Journal of Biomedical Optics, vol. 17, no. 7, p. 077011, 2012.

[18] Y. Hsu, Y. Lin, and W. Hsu, "Learning-based heart rate detection from remote photoplethysmography features," in Proceedings of the 39th ICASSP, Florence, Italy, 2014, pp. 4433–4437.

[19] Y. Sun, S. Hu, V. Azorin-Peris, S. Greenwald, J. Chambers, and Y. Zhu, "Motion-compensated noncontact imaging photoplethysmography to monitor cardiorespiratory status during exercise." Journal of Biomedical Optics, vol. 16, no. 7, p. 077010, 2011.

[20] B. Kim and S. Yoo, "Motion Artifact Reduction in Photoplethysmography Using Independent Component Analysis," IEEE Trans. Biomed. Eng., vol. 53, no. 3, pp. 566–568, 2006.

[21] R. Krishnan, B. Natarajan, and S. Warren, "Two-Stage Approach for Detection and Reduction of Motion Artifacts in Photoplethysmographic Data," IEEE Trans. Biomed. Eng., vol. 57, no. 8, pp. 1867–1876, 2010.

[22] L. Feng, L. Po, X. Xu, and Y. Li, "Motion Artifacts Suppression for Remote Imaging Photoplethysmography," in Proceedings of the 19th DSP, Hong Kong, China, 2014, pp. 18–23.

[23] G. Moody and R. Mark, "A New Method For Detecting Atrial Fibrillation Using RR Intervals," in Proceedings of Computers in Cardiology, Aachen, Germany, 1983, pp. 227–230.

[24] ANSI/AAMI, "American National Standard - Cardiac monitors, heart rate meters, and alarms EC13:2002."

[25] L. Rabiner, "A tutorial on hidden Markov models and selected applications in speech recognition," Proceedings of the IEEE, vol. 77, no. 2, pp. 257–286, 1989.

[26] J. Allen, "Photoplethysmography and its application in clinical physiological measurement," Physiol. Meas., vol. 28, no. 3, pp. R1–39, 2007.